Received February 3, 2013, accepted April 8, 2013, date of publication May 10, 2013, date of current version May 29, 2013.

Digital Object Identifier 10.1109/ACCESS.2013.2260813

Millimeter Wave Mobile Communications for 5G Cellular: It Will Work!

THEODORE S. RAPPAPORT[1], SHU SUN[1], RIMMA MAYZUS[1], HANG ZHAO[1], YANIV AZAR[1], KEVIN WANG[1], GEORGE N. WONG[1], JOCELYN K. SCHULZ[1], MATHEW SAMIMI[1], AND FELIX GUTIERREZ[1]

[1]NYU WIRELESS, Polytechnic Institute of New York University, New York, NY 11201, USA

Corresponding author: T. S. Rappaport (tsr@nyu.edu)

This work was supported by Samsung DMC R&D Communications Research Team and Samsung Telecommunications America, LLC.

ABSTRACT The global bandwidth shortage facing wireless carriers has motivated the exploration of the underutilized millimeter wave (mm-wave) frequency spectrum for future broadband cellular communication networks. There is, however, little knowledge about cellular mm-wave propagation in densely populated indoor and outdoor environments. Obtaining this information is vital for the design and operation of future fifth generation cellular networks that use the mm-wave spectrum. In this paper, we present the motivation for new mm-wave cellular systems, methodology, and hardware for measurements and offer a variety of measurement results that show 28 and 38 GHz frequencies can be used when employing steerable directional antennas at base stations and mobile devices.

INDEX TERMS 28GHz, 38GHz, millimeter wave propagation measurements, directional antennas, channel models, 5G, cellular, mobile communications, MIMO.

I. INTRODUCTION

The rapid increase of mobile data growth and the use of smartphones are creating unprecedented challenges for wireless service providers to overcome a global bandwidth shortage [1], [2]. As today's cellular providers attempt to deliver high quality, low latency video and multimedia applications for wireless devices, they are limited to a carrier frequency spectrum ranging between 700 MHz and 2.6 GHz. As shown in Table 1, the global spectrum bandwidth allocation for all cellular technologies does not exceed 780 MHz, where each major wireless provider has approximately 200 MHz across all of the different cellular bands of spectrum available to them. Servicing legacy users with older inefficient cellphones as well as customers with newer smartphones requires simultaneous management of multiple technologies in the same band-limited spectrum. Currently, allotted spectrum for operators is dissected into disjoint frequency bands, each of which possesses different radio networks with different propagation characteristics and building penetration losses. This means that base station designs must service many different bands with different cell sites, where each site has multiple base stations (one for each frequency or technology usage e.g. third generation (3G), fourth generation (4G), and Long Term Evolution - Advanced (LTE-A)) [3], [4]. To procure new spectrum, it can take a decade of administration through regulatory bodies such as the International Telecommunication Union (ITU) and the U.S. Federal Communications Commission (FCC). When spectrum is finally licensed, incumbent users must be moved off the spectrum, causing further delays and increasing costs.

TABLE 1. Current 2G, 3G, 4G, & LTE-A spectrum and bandwidth allocations [5].

Band	Uplink (MHz)	Downlink (MHz)	Carrier Bandwidth (MHz)
700 MHz	746-763	776-793	1.25 5 10 15 20
AWS	1710-1755	2110-2155	1.25 5 10 15 20
IMT Extension	2500-2570	2620-2690	1.25 5 10 15 20
GSM 900	880-915	925-960	1.25 5 10 15 20
UMTS Core	1920-1980	2110-2170	1.25 5 10 15 20
GSM 1800	1710-1785	1805-1880	1.25 5 10 15 20
PCS 1900	1850-1910	1930-1990	1.25 5 10 15 20
Cellular 850	824-849	869-894	1.25 5 10 15 20
Digital Dividend	470-854		1.25 5 10 15 20

2169-3536/$31.00 © 2013 IEEE

MASSIVELY BROADBAND, IPR2025-01563, Ex.2013, Page 1 of 15

Mobile broadband networks need to support ever-growing consumer data rate demands and will need to tackle the exponential increase in the predicted traffic volumes. An efficient radio access technology combined with more spectrum availability is essential to achieve the ongoing demands faced by wireless carriers.

A. THE WIRELESS EVOLUTION

To date, four generations of cellular communication systems have been adopted in the USA with each new mobile generation emerging every 10 years or so since around 1980: first generation analog FM cellular systems in 1981; second generation digital technology in 1992, 3G in 2001, and 4G LTE-A in 2011 [6]. The evolution from 1G to 4G is summarized in Table 2.

TABLE 2. Requirements and realities of 1G through 4G cellular systems [7].

Generation	Requirements	Comments
1G	No official requirements. Analog technology.	Deployed in the 1980s.
2G	No official requirements. Digital Technology.	First digital systems. Deployed in the 1990s. New services such as SMS and low-rate data. Primary technologies include IS-95 CDMA and GSM.
3G	ITU's IMT-2000 required 144 kbps mobile, 384 kbps pedestrian, 2 Mbps indoors	Primary technologies include CDMA2000 1X/EV-DO and UMTS-HSPA. WiMAX now an official 3G technology.
4G	ITU's IMT-Advanced requirements include ability to operate in up to 40 MHz radio channels and with very high spectral efficiency.	No technology meets requirements today. IEEE 802.16m and LTE-Advanced being designed to meet requirements.

First generation cellular networks were basic analog systems designed for voice communications. A move to early data services and improved spectral efficiency was realized in 2G systems through the use of digital modulations and time division or code division multiple access. 3G introduced high-speed Internet access, highly improved video and audio streaming capabilities by using technologies such as Wideband Code Division Multiple Access (W-CDMA) and High Speed Packet Access (HSPA). HSPA is an amalgamation of two mobile telephony protocols, High Speed Downlink Packet Access (HSDPA) and High Speed Uplink Packet Access (HSUPA), which extends and improves the performance of existing 3G mobile telecommunication networks utilizing WCDMA protocols. An improved 3GPP (3rd Generation Partnership Project) standard, Evolved HSPA (also known as HSPA+), was released in late 2008 with subsequent worldwide utilization beginning in 2010. HSPA has been deployed in over 150 countries by more than 350 communications service providers (CSP) on multiple frequency bands and is now the most extensively sold radio technology worldwide [8], although LTE is closing the gap rapidly.

The International Mobile Telecommunications-Advanced (IMT-Advanced) standard is the next-generation of mobile communications technology defined by the ITU and includes capabilities outstripping those of IMT-2000 (3G) mobile communication. ITU refers to IMT-Advanced as a 4G mobile communications technology, although it should be noted that there is no universally accepted definition of the term 4G. LTE radio access technology has been developed by the 3GPP to offer a fully 4G-capable mobile broadband platform [9]. LTE is an orthogonal frequency-division multiplexing (OFDM)-based radio access technology that supports a scalable transmission bandwidth up to 20 MHz and advanced multi-antenna transmission. As a key technology in supporting high data rates in 4G systems, Multiple-Input Multiple-Output (MIMO) enables multi-stream transmission for high spectrum efficiency, improved link quality, and adaptation of radiation patterns for signal gain and interference mitigation via adaptive beamforming using antenna arrays [10]–[12]. The coalescence of HSPA and LTE will increase the peak mobile data rates of the two systems, with data rates exceeding 100 Mbps, and will also allow for optimal dynamic load balancing between the two technologies [8].

As the demand for capacity in mobile broadband communications increases dramatically every year, wireless carriers must be prepared to support up to a thousand-fold increase in total mobile traffic by 2020, requiring researchers to seek greater capacity and to find new wireless spectrum beyond the 4G standard [13]. To improve the existing LTE network, the wireless technology roadmap now extends to IMT-Advanced with LTE-Advanced defined to meet IMT-Advanced requirements, which will be theoretically capable of peak throughput rates that exceed 1 Gigabit per second (Gbps). LTE-Advanced supports heterogeneous networks with co-existing large macro, micro, and pico cells, and Wi-Fi access points. Low cost deployment will be realized by self-organizing features and repeaters/relays

As fifth generation (5G) is developed and implemented, we believe the main differences compared to 4G will be the use of much greater spectrum allocations at untapped mm-wave frequency bands, highly directional beamforming antennas at both the mobile device and base station, longer battery life, lower outage probability, much higher bit rates in larger portions of the coverage area, lower infrastructure costs, and higher aggregate capacity for many simultaneous users in both licensed and unlicensed spectrum (e.g. the convergence of Wi-Fi and cellular). The backbone networks of 5G will move from copper and fiber to mm-wave wireless connections, allowing rapid deployment and mesh-like connectivity with cooperation between base stations.

B. EARLY GLOBAL ACTIVITIES FOR Beyond 4G (B4G) AND 5G WIRELESS

The evolution of wireless communication systems requires global collaboration, involving worldwide mobile communication companies and governments. The Electronics and Telecommunication Research Institute (ETRI) in Korea has actively contributed to the development of 4G systems. In 2002, the Mobile Communication Research Laboratory

MASSIVELY BROADBAND, IPR2025-01563, Ex.2013, Page 2 of 15

(MCRL) of ETRI initiated the R&D of the 4G radio transmission system for HSPA and proposed their vision of 4G radio mobile communications [14]. According to ETRI, the 4G system would satisfy the data rate requirement of 100 Mbps for high mobility with Systems Beyond IMT-2000 (SBIMT) and would provide high quality service for both low-tier and high-tier cellular systems.

In the early 2000s, aiming at integrating voice and web data in an IP-based mobile communications system (i.e. 4G wireless network), Sun Microsystems engineers were designing and implementing mobile IP-based protocols and tools to implement secure, versatile and responsive wireless communication technologies [15], [16].

A memorandum of understanding (MoU) was signed by the government of Karnataka in India with Charmed Technologies Inc. from Beverly Hills, California, and Software Technology Parks of India in Karnataka to develop "4G" wireless technology in the year 2001 [17].

In 2005, Samsung envisaged the increasing demands of higher data rates, and the eventual convergence of digital multimedia and ubiquitous computing [18]. Samsung's 4G vision has mainly focused on digital convergence including implementations of bi-directional HDTV, increasing e-health and e-education services, and ubiquitous wireless network services. With an evolution from fixed broadband to mobile broadband, more converged, personalized, convenient and seamless secure services will be achieved, and Samsung has recently made contributions in the area of mm-wave wireless [2], [12].

Recently, Korea has carried out a series of R&D activities toward beyond 4G evolution [19]. It aims to establish "Giga Korea" during 2013 to 2020 for hyper connected IT infrastructure deployment. Those activities include the acquisition of wider spectrum, green networks and devices, special purpose networks, and new network topologies and media [19].

Nokia Siemens Networks (NSN) has conducted research activities in radio, together with industry and research partners, making contributions to the 3GPP LTE standard. NSN believes that with improvement in digital processing power, radio implementation bandwidth, and the availability of optical fiber, the radio evolution will continue. The next evolutionary stage, beyond 4G, is likely to support up to 1,000 times higher traffic volumes than 2010 traffic levels, with peak and cell edge rates higher than 10 Gbps and 100 Mbps respectively with latency less than 1 ms for local area networks [20], and will realize wide scale small cell (heterogeneous) deployments, fast interference coordination and cancellation, Cognitive Radio Networks (CRNs), and Self Organizing Networks (SONs) [13]. Further, future networks may require the combinations of diverse radio access technologies such as LTE, HSPA, Wi-Fi, and B4G [13].

The University of Surrey, England, has set up a world research hub for 5G mobile technology with a goal to expand UK telecommunication research and innovation [21]. New York University (NYU) and NYU-Poly recently established the NYU WIRELESS research center, to create new technologies and fundamental knowledge for future mm-wave wireless devices and networks [36].

C. A MILLIMETER WAVE SOLUTION FOR FUTURE 5G CELLULAR NETWORKS

Despite industrial research efforts to deploy the most efficient wireless technologies possible, the wireless industry always eventually faces overwhelming capacity demands for its currently deployed wireless technologies, brought on by the continued advances and discoveries in computing and communications, and the emergence of new customer handsets and use cases (such as the need to access the internet). This trend will occur in the coming years for 4G LTE, implying that at some point around 2020, wireless networks will face congestion, as well as the need to implement new technologies and architectures to properly serve the continuing demands of carriers and customers. The life cycle of every new generation of cellular technology is generally a decade or less (as shown earlier), due to the natural evolution of computer and communications technology. Our work contemplates a wireless future where mobile data rates expand to the multi gigabit-per-second range, made possible by the use of steerable antennas and mm-wave spectrum that could simultaneously support mobile communications and backhaul, with the possible convergence of cellular and Wi-Fi services.

Recent studies suggest that mm-wave frequencies could be used to augment the currently saturated 700 MHz to 2.6 GHz radio spectrum bands for wireless communications [2]. The combination of cost-effective CMOS technology that can now operate well into the mm-wave frequency bands, and high-gain, steerable antennas at the mobile and base station, strengthens the viability of mm-wave wireless communications [22], [23] Further, mm-wave carrier frequencies allow for larger bandwidth allocations, which translate directly to higher data transfer rates. Mm-wave spectrum would allow service providers to significantly expand the channel bandwidths far beyond the present 20 MHz channels used by 4G customers [1]. By increasing the RF channel bandwidth for mobile radio channels, the data capacity is greatly increased, while the latency for digital traffic is greatly decreased, thus supporting much better internet-based access and applications that require minimal latency. Mm-wave frequencies, due to the much smaller wavelength, may exploit polarization and new spatial processing techniques, such as massive MIMO and adaptive beamforming [24]. Given this significant jump in bandwidth and new capabilities offered by mm-waves, the base station-to-device links, as well as backhaul links between base stations, will be able to handle much greater capacity than today's 4G networks in highly populated areas. Also, as operators continue to reduce cell coverage areas to exploit spatial reuse, and implement new cooperative architectures such as cooperative MIMO, relays, and interference mitigation between base stations, the cost per base station will drop as they become more plentiful and more densely distributed in urban areas, making wireless backhaul

MASSIVELY BROADBAND, IPR2025-01563, Ex.2013, Page 3 of 15

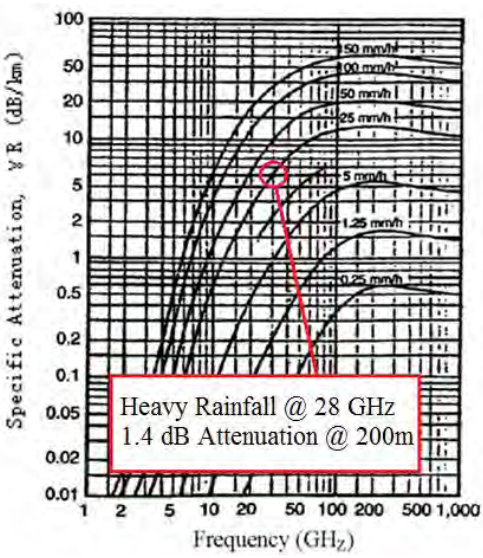

FIGURE 1. Rain attenuation in dB/km across frequency at various rainfall rates [26]. The rain attenuation at 28 GHz has an attenuation of 7 dB/km for a very heavy rainfall of 25 mm/hr (about 1 inch per hour). If cell coverage regions are 200 m in radius, the rain attenuation will reduce to 1.4 dB.

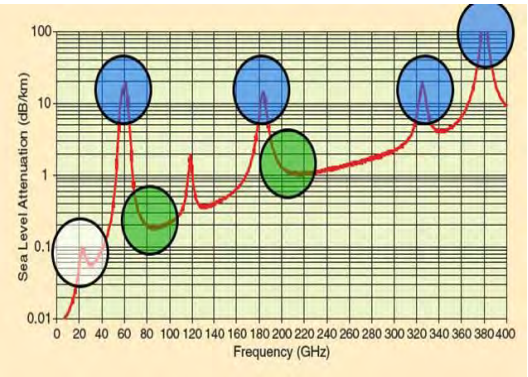

FIGURE 2. Atmospheric absorption across mm-wave frequencies in dB/km [1]. The attenuation caused by atmospheric absorption is 0.012 dB over 200 m at 28 GHz and 0.016 dB over 200 m at 38 GHz. Frequencies from 70 to 100 GHz and 125 to 160 GHz also have small loss.

essential for flexibility, quick deployment, and reduced ongoing operating costs. Finally, as opposed to the disjointed spectrum employed by many cellular operators today, where the coverage distances of cell sites vary widely over three octaves of frequency between 700 MHz and 2.6 GHz, the mm-wave spectrum will have spectral allocations that are relatively much closer together, making the propagation characteristics of different mm-wave bands much more comparable and "homogenous". The 28 GHz and 38 GHz bands are currently available with spectrum allocations of over 1 GHz of bandwidth. Originally intended for Local Multipoint Distribution Service (LMDS) use in the late 1990's, these licensees could be used for mobile cellular as well as backhaul [25].

A common myth in the wireless engineering community is that rain and atmosphere make mm-wave spectrum useless for mobile communications. However, when one considers the fact that today's cell sizes in urban environments are on the order of 200 m, it becomes clear that mm-wave cellular can overcome these issues. Fig. 1 and Fig. 2 show the rain attenuation and atmospheric absorption characteristics of mm-wave propagation. It can be seen that for cell sizes on the order of 200 m, atmospheric absorption does not create significant additional path loss for mm-waves, particularly at 28 GHz and 38 GHz. Only 7 dB/km of attenuation is expected due to heavy rainfall rates of 1 inch/hr for cellular propagation at 28 GHz, which translates to only 1.4 dB of attenuation over 200 m distance. Work by many researchers has confirmed that for small distances (less than 1 km), rain attenuation will present a minimal effect on the propagation of mm-waves at 28 GHz to 38 GHz for small cells [26].

D. Mm-WAVE CELLULAR MEASUREMENTS: UNDERSTANDING THE CHANNEL

Future wireless technologies must be validated in the most urban environments, such as New York City. In order to improve capacity and service quality, the cellular network architecture needs to support higher spatial reuse. Massive MIMO base stations and small-cell access points are two promising approaches for future cellular. Massive MIMO base stations allocate antenna arrays at existing macro base stations, which can accurately concentrate transmitted energy to the mobile users [24]. Small cells offload traffic from base stations by overlaying a layer of small cell access points, which actually decreases the average distance between transmitters and users, resulting in lower propagation losses and higher data rates and energy efficiency [24]. Both of these important trends are readily supported and, in fact, are enhanced by a move to mm-wave spectrum, since the tiny wavelengths allow for dozens to hundreds of antenna elements to be placed in an array on a relatively small physical platform at the base station, or access point, and the natural evolution to small cells ensures that mm-wave frequencies will overcome any attenuation due to rain.

Understanding the radio channel is a fundamental requirement to develop future mm-wave mobile systems as well as backhaul techniques. With a firm technical understanding of the channel, researchers and industry practitioners may then explore new methods for the air interface, multiple access, architectural approaches that include cooperation and interference mitigation and other signal enhancement techniques. In order to create a statistical spatial channel model (SSCM) for mm-wave multipath channels, extensive measurements must be made in typical and worst-case operating conditions and environments. We have conducted extensive propagation measurements in urban environments in New York City and suburban environments in Austin, Texas in order to understand the mm-wave channel.

MASSIVELY BROADBAND, IPR2025-01563, Ex.2013, Page 4 of 15

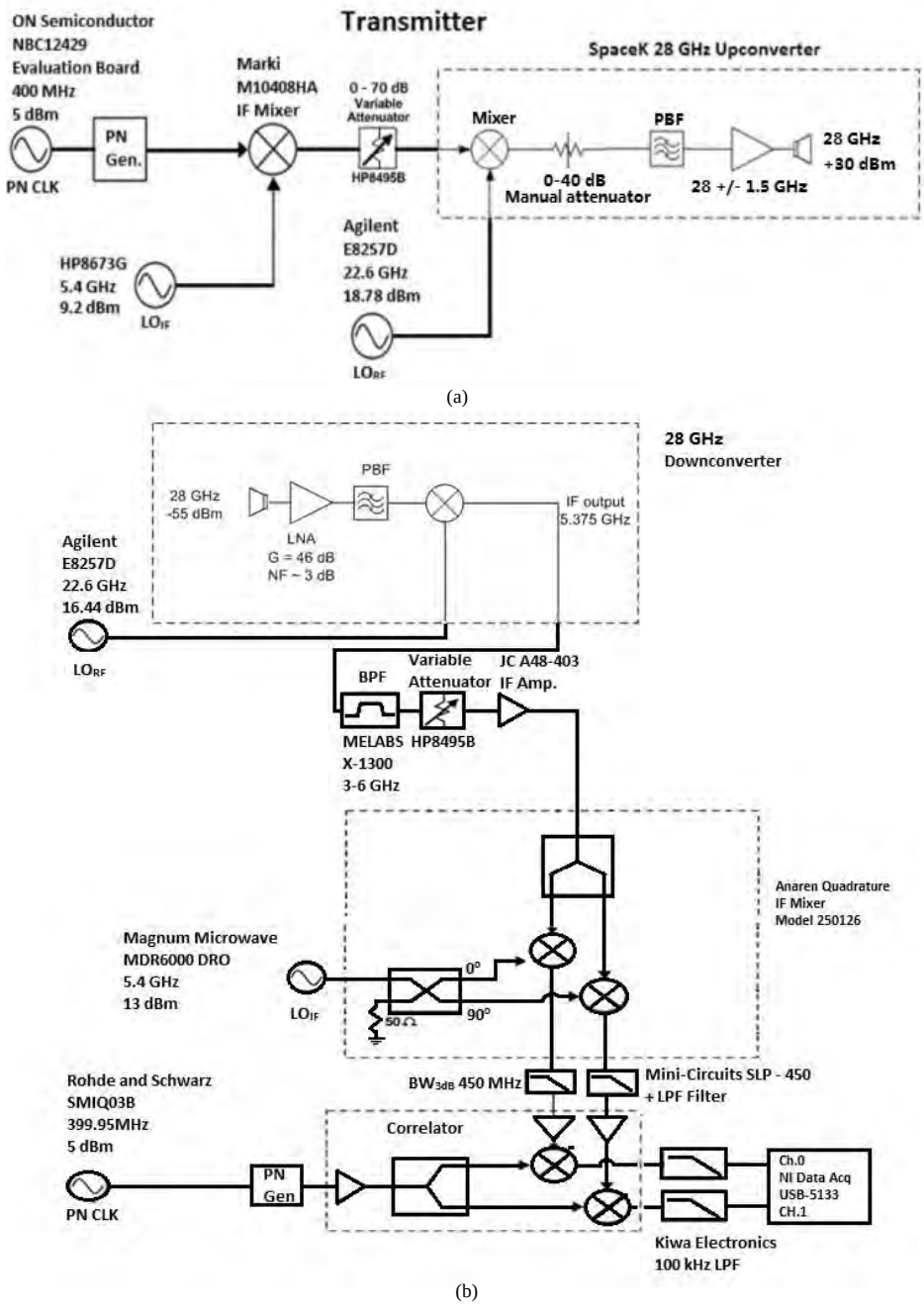

FIGURE 3. Block diagram of the (a) TX and (b) RX for the mm-wave propagation measurements at 28 GHz in New York City.

II. 28 GHZ BUILDING PENETRATION AND REFLECTION CAMPAIGN IN NEW YORK CITY

A. 28 GHZ BROADBAND CHANNEL SOUNDING HARDWARE

Using a 400 Mcps sliding correlator channel sounder with 2.3 ns multipath resolution, we conducted extensive mm-wave propagation measurements at 28 GHz in New York City in 2012. The block diagram of the transmitter (TX) and receiver (RX) is given in Fig. 3. A pseudo-random noise (PN) sequence sliding correlator was utilized as the probing signal, which was modulated to a 5.4 GHz intermediate frequency (IF) and upconverted to 28 GHz after mixing with a 22.6 GHz local oscillator (LO), in a manner similar to [27]. The transmitter power was +30 dBm (a typical value for lower power femtocells), fed to a steerable 10° beamwidth 24.5 dBi horn antenna or a 30° beamwidth 15 dBi horn antenna that was mechanically rotated. The receiver used the

MASSIVELY BROADBAND, IPR2025-01563, Ex.2013, Page 5 of 15

TABLE 3. Summary of penetration losses through various common building materials at 28 GHz. Both of the horn antennas have 24.5 dBi gains with 10° half power beamwidth [28].

Environment	Location	Material	Thickness (cm)	Received Power - Free Space (dBm)	Received Power - Material (dBm)	Penetration Loss (dB)
Outdoor	ORH	Tinted Glass	3.8	-34.9	-75.0	40.1
	WWH	Brick	185.4	-34.7	-63.1	28.3
Indoor	MTC	Clear Glass	<1.3	-35.0	-38.9	3.9
	WWH	Tinted Glass	<1.3	-34.7	-59.2	24.5
		Clear Glass	<1.3	-34.7	-38.3	3.6
		Wall	38.1	-34.0	-40.9	6.8

TABLE 4. Penetration losses for multiple indoor obstructions in an office environment at 28 GHz. Weak signals are denoted by locations where the SNR was high enough to distinguish signal from noise but not enough for the signal to be acquired, i.e. penetration losses were between 64 dB to 74 dB relative to a 5 m free space test. No signal detected denotes an outage, where penetration loss is greater than 74 dB relative to a 5 m free space test [28].

RX ID	TX-RX Separation (m)	# of Partitions				Transmitted Power (dBm)	Power Received – Free Space (dBm)	Received Power – Test Material (dBm)	Penetration Loss (dB)
		Wall	Door	Cubicles	Elevator				
1	4.7	2	0	0	0	-8.6	-34.4	-58.8	24.4
2	7.8	3	0	0	0	-8.6	-38.7	-79.8	41.1
3	11.4	3	1	0	0	11.6	-21.9	-67.0	45.1
5	25.6	4	0	2	0	21.4	-19.0	-64.1	45.1
4	30.1	3	2	0	0	21.4	-30.4	Weak Signal Detected	
6	30.7	4	0	2	0	21.4	-30.5		
7	32.2	5	2	2	0	21.4	-30.9		
8	35.8	5	0	2	1	21.4	-31.9	No Signal Detected	

TABLE 5. Comparison of reflection coefficients for various common building materials at 28 GHz. Both of the horn antennas have 24.5 dBi gains with 10° half power beamwidth [28].

Environment	Location	Material	Angle (°)	Reflection Coefficient ($\lvert\Gamma_{\parallel}\rvert$)
Outdoor	ORH	Tinted Glass	10	0.896
		Concrete	10	0.815
			45	0.623
Indoor	MTC	Clear Glass	10	0.740
		Drywall	10	0.704
			45	0.628

same type of horn antennas as the transmitter. In order to achieve increased measurement dynamic range for increased coverage distance, we used a sliding correlator spread spectrum system [5]. Total measured dynamic range was approximately 178 dB between the transmitter and receiver using the most directional horn antennas in order to obtain an SNR of 10 dB, on the order of future small cells. All propagation measurement equipment used AC power outlets that were available from various buildings, thus avoiding any battery depletion problem.

B. 28 GHz BUILDING PENETRATION AND REFLECTION MEASUREMENT

To understand the mm-wave propagation environment in urban areas, signal penetration and reflection properties of common building materials with typical smooth and rough surfaces are required for both indoor and outdoor cases [26]. We conducted penetration and reflection measurements at 28 GHz throughout the summer of 2012 in New York City [28]. Penetration and reflection measurements for common materials were conducted at three locations at the NYU campus in New York City: (a) the 10th floor of 2 MetroTech Center (MTC) in Brooklyn, (b) the Othmer Residence Hall (ORH) in Brooklyn, and (c) Warren Weaver Hall (WWH) in Manhattan [28]. The block diagram of the channel sounding hardware used in this campaign is shown in Fig. 3.

Penetration losses through building materials were collected by first performing a 5-meter free space reference measurement resulting in 75.3 dB path loss, and then positioning the TX and RX on opposite sides of the test material at the

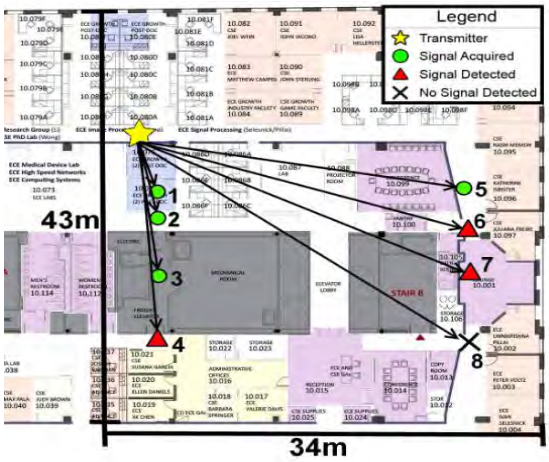

FIGURE 4. Map of the penetration measurements through multiple obstructions in an office environment located at the 10th floor of 2 MetroTech Center in Brooklyn, New York. The TX location is represented by a yellow star, the RX locations where signals can be acquired are represented by green circles, and the RX locations where weak signals can be detected are in red triangles. The black cross denotes an outage [28].

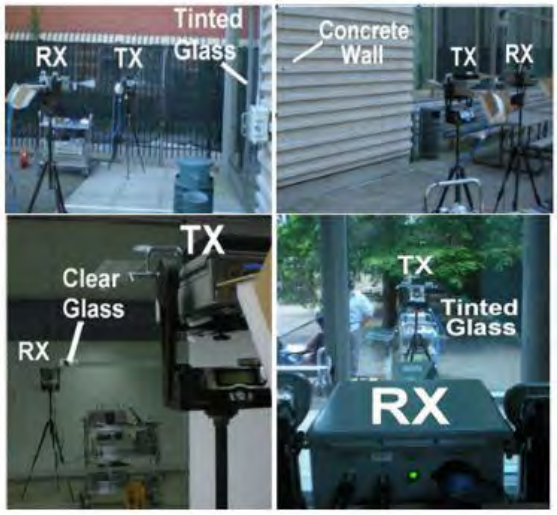

FIGURE 5. Images of the 28 GHz reflection measurement for outdoor tinted glass at ORH (top left), outdoor concrete wall at ORH (top right), penetration loss measurement for indoor clear non-tinted glass at MTC (bottom left) and tinted glass at ORH (bottom right) [28].

same distance. Materials tested for penetration loss include: tinted glass, brick, clear non-tinted glass, and drywall. Table 3 summarizes the penetration loss results for these common building materials [28]. As shown in Table 3, tinted glass and brick pillars (typical exterior surfaces of urban buildings) have high penetration losses of 40.1 dB and 28.3 dB, respectively. This illustrates the fact that building penetration of mm-waves will be difficult for outdoor transmitters, thus providing high isolation between outdoor and indoor networks. On the other hand, common indoor materials such as clear non-tinted glass and drywall only have 3.6 dB and 6.8 dB of losses, respectively, which are relatively low.

In addition to penetration measurements for individual materials, penetration measurements were also made through multiple obstructions in typical office environments, to determine overall average partition losses, as was done in [29] using "primary ray tracing" where a single ray is drawn between the TX and RX, and attenuations of obstructions are determined through measurements. As shown in Fig. 4, multiple indoor obstructions in an office building environment were characterized using 8 RX locations, in which each RX location was selected to determine penetration through increasing layers of obstructions. Partition layers included multiple walls, doors, cubicles, and an elevator bank (RX 8) [28]. We used lower TX power which limited the maximum measurable path loss to about 169 dB.

Table 4 presents a summary of the number and type of obstructions between the TX and RX, as well as the 28 GHz penetration loss results caused by multiple obstructions in a typical office environment. Note that the RX locations are ordered in increasing TX-RX separation distances. Data is grouped into three subsections: signal acquired (with values listed), signal detected, and no signal detected. Signal acquired is defined as a location where the SNR is sufficiently high for accurate acquisition, i.e. penetration loss relative to 5 meters free space test is less than 64 dB. Signal detected is a location where the SNR is high enough to slightly distinguish a signal from noise but not strong enough to be acquired, i.e. penetration loss between 64 dB to 74 dB relative to a 5 m free space test. No signal detected denotes an outage, where the penetration loss is at least 74 dB greater than the 5 m free space test. As shown in Table 4, penetration loss does not greatly depend on the TX-RX separation distance, but mostly depends on the number and type of obstructions. The RX sites with TX-RX separation distances of 25.6 m and 11.4 m have virtually identical measured penetration losses of 45.1 dB; however, the site with 25.6 m separation distance has obstructions of four walls and two cubicles while the other site with 11.4 m separation distance has obstructions of three walls and one door. Note that one outage was found at the RX site with a separation distance of 35.8 m, a result of the large separation distance and the inability of RF waves to penetrate the metallic elevator bank.

Table 5 summarizes and compares the reflection coefficients for common indoor and outdoor building materials. As indicated in Table 5, the outdoor materials have larger reflection coefficients of 0.896 for tinted glass and 0.815 for concrete at a 10° incident angle, as compared to clear non-tinted glass and drywall, which have lower reflection coefficients of 0.740 and 0.704, respectively. The results for outdoor tinted glass in ORH consistently show that a large portion of the signal (= 0.896) is reflected and could not penetrate through the glass. In contrast, the clear non-tinted glass located inside the MTC building has a smaller reflection coefficient (= 0.740) and causes only 3.9 dB of penetration loss compared to the 40.1 dB loss for the outdoor tinted glass in ORH. The high penetration loss through outdoor building materials and low attenuation through indoor materials suggest that RF energy can be contained in intended areas within

MASSIVELY BROADBAND, IPR2025-01563, Ex.2013, Page 7 of 15

buildings which reduces interference, yet making outdoor-to-indoor building penetration more difficult. Fig. 5 presents photographs of the penetration and reflection measurements of common building materials at 28 GHz.

III. 28 GHz URBAN PROPAGATION CAMPAIGN IN NEW YORK CITY

A. MEASUREMENT PROCEDURE

The hardware system of Fig, 3 was used in the outdoor propagation measurement campaign in New York City. We selected one TX and 11 RX measurement locations at the NYU-Poly campus in downtown Brooklyn. The distance between the TX and RX ranged from 75 m to 125 m. At the NYU campus in Manhattan, 3 TX and 75 RX locations (with 25 RX sites for each TX site) were chosen with TX-RX separations varying from 19 m to 425 m to emulate future cellular base stations. At three of the measurement locations in Brooklyn, the RX was moved on an automated linear track of 10 wavelengths (107 mm) in half-wavelength (5.35mm) increments to study small scale signal level variations, i.e. small scale fading. At each track position, a 360° azimuthal sweep was performed in steps of 10° (if using the 10° beamwidth 24.5 dBi narrow-beam horn antenna), or 30° (if using the 30° beamwidth 15 dBi wide-beam horn antenna). Large scale propagation characteristics were investigated in the remaining eight RX locations in Brooklyn and all the Manhattan measurements using 24.5 dBi narrow beam antennas. At each TX and RX location, extensive measurements were conducted for three different TX azimuth angles, −5° , 0° , and +5° from boresight to the receiver, and for three different RX elevation angles of −20° , 0° , and +20° creating nine possible antenna pointing combinations between TX and RX. For each of the nine antenna pointing combinations, the RX antenna was swept 360° in the azimuth plane in 10° steps, and measurements were recorded if energy was received. Finally, cross polarization measurements were done at all Brooklyn RX sites where both vertical and horizontal electric polarization fields were measured.

Propagation measurements were conducted in New York City around the NYU campuses in Manhattan and Brooklyn. Each location had the potential to collect 324 power delay profiles (PDPs) for all combinations (36 RX azimuth angles, 3 TX azimuth angles, and 3 RX elevation angles). Not all azimuth angles yielded a detectable signal.

B. PATH LOSS AND SIGNAL OUTAGE ANALYSIS

Given the highly reflective outdoor environment, PDPs displayed numerous multipath with large excess delay for both line-of sight (LOS) and non-line-of-sight (NLOS) environments. The average number of resolvable multipath components in a LOS environment was 7.2 with a standard deviation of 2.2 for a TX-RX separation of less than 200 meters. NLOS measurements with TX-RX separation less than 100 meters showed that the number of average received multipath components is 6.8 with a standard deviation equal to that of a LOS case. With a 52 meter separation, in a LOS environment,

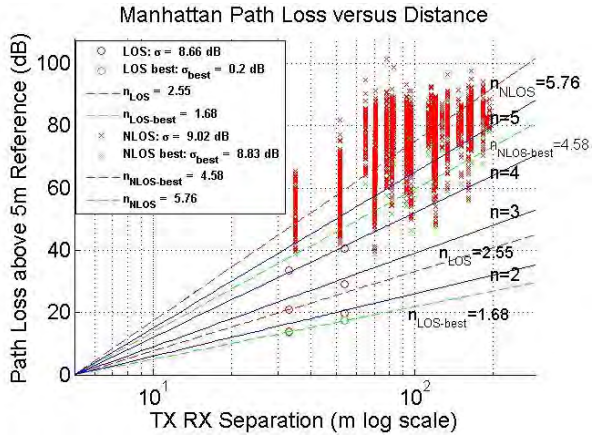

FIGURE 6. Measured path loss values relative to 5 m free space path loss for 28 GHz outdoor cellular channels. These path loss values were measured using a 24.5 dBi narrow beam antenna. The antennas were rotated in the azimuth plane, recording measurements at 10° incremental steps. The values in the legend represent the PLE of each environment (LOS and NLOS) [31].

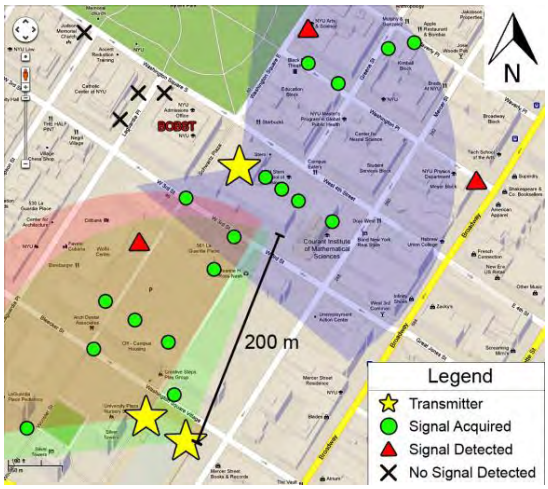

FIGURE 7. Map showing all Manhattan coverage cells with radii of 200 m and their different sectors. Measurements were recorded for each of the 25 RX sites from each of the three TX sites (yellow stars). Signal Acquired means that signal was detected and acquired. Signal Detected means that signal was detected, but low SNR prevented data acquisition by the system [31].

a large 753.5 ns excess delay was observed, and a NLOS excess delay over 423 meters extended to 1388.4 ns. While these results were not commonly observed, these cases are evidence that enough signal strength can propagate through a highly reflective environment over a long distance to create a TX-RX link. When path loss was calculated for all locations, the best LOS path loss exponent (PLE) was n = 1.68 (here "best" means "smallest"). The LOS PLE resulting from all the measurements acquired in New York City was n = 2.55 (which included many cases where the TX and RX had an optical LOS environment between them but the directional antennas were not precisely lined up on boresight). The average PLE over all NLOS locations increased to n = 5.76, as

MASSIVELY BROADBAND, IPR2025-01563, Ex.2013, Page 8 of 15

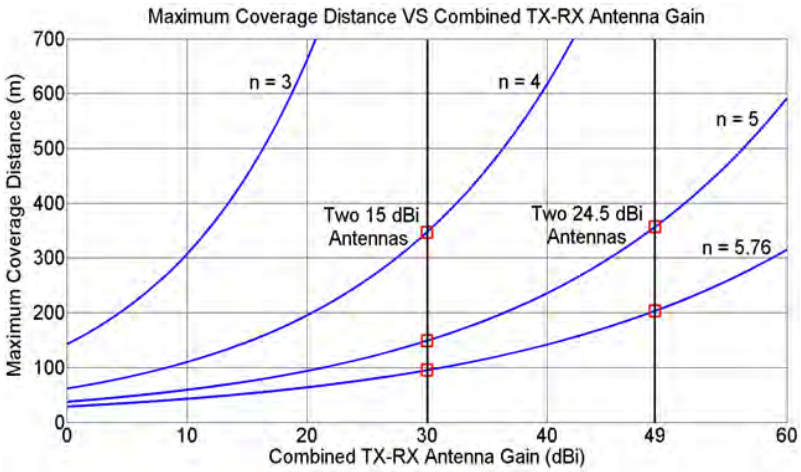

FIGURE 8. Maximum coverage distance at 28 GHz with 119 dB maximum path loss dynamic range without antenna gains and 10 dB SNR, as a function of path loss exponent n.

shown in Fig. 6. However, the NLOS PLE was significantly reduced when pointing the TX and RX directional antennas to the best angle combination at each RX location, resulting in an average "best" NLOS PLE of n = 4.58, an improvement of 11.8 dB/decade in path loss, which is significant to cellular providers for range extension. By finding the best antenna orientations at any location, the NLOS PLE of n = 4.58 is virtually identical to NLOS path loss experienced in today's 700 MHz ∼ 2.6 GHz bands [30].

An outage study was conducted in Manhattan, New York, to find the locations and distances where energy could not be detected [31]. As seen in Fig. 7, the map is sectioned into sectors corresponding to TX locations. Signal acquired by the RX for all cases was within 200 meters. While most of the RX locations within the range of 200 meters from the TX detected a signal, in some instances, signal-to-noise ratio (SNR) was not high enough for a signal to be acquired by the hardware. Of the measurements taken in Manhattan, it was found that 57% of locations were outages due to the obstructive nature of the channel with most outages occurring beyond 200 m from the TX.

The outage probability is greatly affected by the transmitted power, antenna gains as well as the propagation environment. Fig. 8 displays the relationship between the maximum coverage distance of the base station and the combined TX-RX antenna gain. To calculate the maximum coverage distance, we subtracted the 49 dBi combined antenna gain from the total measurable path loss of 178 dB (which was obtained using the two 24.5 dBi antennas), resulting in the dynamic range without the antenna gain. Since our system requires approximately 10 dB SNR for a reliable detecting level, the actual maximum measureable path loss is 119 dB without including antenna gains, and this was used to compute the coverage distances corresponding to various antenna gains. The four blue curves denote the cases for PLEs equal to 3, 4, 5 and 5.76. The red squares in Fig. 8 highlight the coverage distance corresponding to the two 15 dBi horn antennas and 24.5 dBi horn antennas at the TX and RX. Obviously, the maximum coverage distance increases with increasing antenna gains and a decrease of the PLE. For example, the radio waves can propagate about 200 m in a highly obstructed environment with a PLE of 5.76 when the combined TX-RX antenna gain is 49 dBi, which agrees with our measured values (200 m) very well. This suggests that we can enlarge the coverage region of a base station by increasing antenna gains, and may use less antenna gain (or TX power) when in LOS conditions.

C. 28 GHz AOA AND AOD ANALYSIS

By employing highly directional steerable horn antennas to simulate an antenna array, we were able to obtain angle of arrival (AOA) and angle of departure (AOD) data necessary to determine the multipath angular spread at the transmitter for AOD and at the receiver for AOA. By completing a 360° exhaustive sweep of the TX and RX antennas, we were able to determine the angles with the highest received power. Data collected at environments classified as LOS, partially obstructed LOS, and NLOS provide a basis for the development of a spatial channel model. The path loss and root mean squared (RMS) delay spreads can be used to accurately characterize the channel [31].

Fig. 9 demonstrates a polar plot of received power at the RX on the corner of Greene and Broadway in downtown Manhattan, a location categorized as a NLOS environment. The distance between the TX and RX was 78 m. In the figure, each dot represents the received power level in dBm (denoted on the radius of the polar plot) at the corresponding RX azimuth angle. The number of resolvable multipath components, path loss in dB with respect to the 5 m free space reference, and RMS delay spread in nanoseconds are displayed from left to right on the periphery of the plot. As can be seen, TX-RX links were successfully established

MASSIVELY BROADBAND, IPR2025-01563, Ex.2013, Page 9 of 15

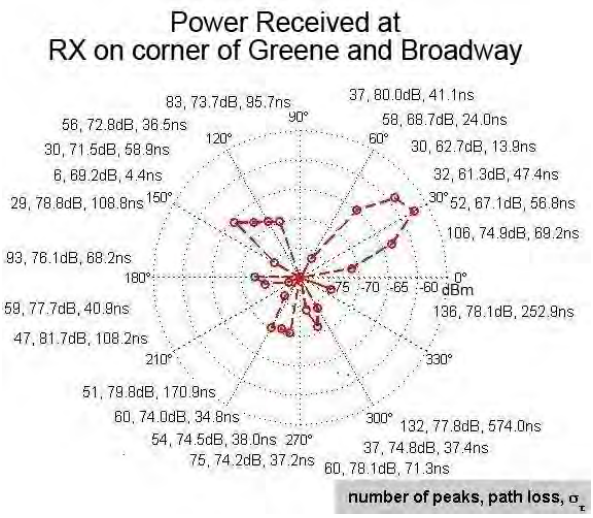

FIGURE 9. **Polar plot showing the received power at a NLOS location. This plot shows an AOA measurement at the RX on Greene and Broadway from the TX on the five-story Kaufman building (78 m T-R separation). The polar plot shows the received power in dBm, the number of resolvable multipath components, the path loss in dB with respect to the 5 m free space reference, and RMS delay spread with varying RX azimuth angles [31].**

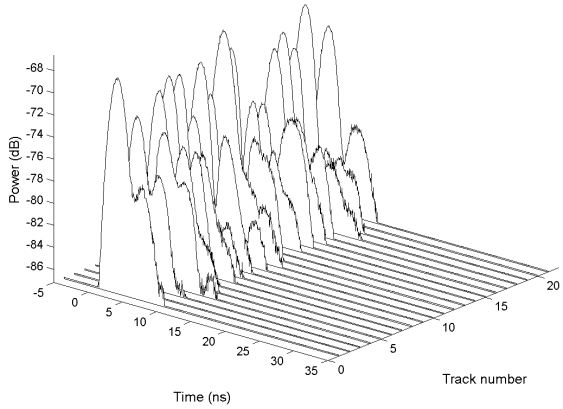

FIGURE 10. **Power delay profiles measured over a 10-wavelength linear track at 28 GHz. The RX was 135 meters away from the TX. The TX and RX were pointed for maximum signal power. Track step size was half wavelength using 24.5 dBi horn antennas with beamwidths of 10.9° on the TX and RX.**

at 22 out of 36 RX azimuth angles. Furthermore, it is obvious that a wealth of multipath components exist at numerous different pointing angles, providing great diversity which can be utilized for beam combining and link improvement in future 5G systems.

Small scale fading has also been explored by moving the RX at half-wavelength (5.35 mm) increments along a small scale linear track of 10 wavelengths (107 mm), while the TX was fixed at a certain location [32]. Fig. 10 shows the 3D power delay profiles of small scale fading for the TX-RX angle combination for the strongest received power. The maximum and minimum received signal powers were −68 dBm/ns and −74 dBm/ns, respectively, yielding merely ±3 dB fading variation. This outcome indicates that movements over the small scale track exert little influence on the AOA or the received power level of multipath signals.

IV. 38 GHz CELLULAR URBAN PROPAGATION CAMPAIGN IN AUSTIN

A. 38 GHz BROADBAND CHANNEL SOUNDING HARDWARE AND MEASUREMENT PROCEDURE

An 800 MHz null-to-null bandwidth spread spectrum sliding correlator channel sounder was employed in the 38 GHz propagation measurement campaign in Austin. The PN sequence was operating at 400 Mcps and 399.9Mcps at the TX and RX, respectively, to offer a slide factor of 8000 and adequate processing gain [33]. The PN sequence was modulated by a 5.4 GHz IF signal, which was input into the upconverter that contained LO frequency multipliers to generate a carrier frequency of 37.625 GHz with a +22 dBm output power before the TX antenna. A 25-dBi gain Ka-band vertically polarized horn antenna with 7.8° half-power beamwidth was utilized at the TX, and an identical antenna (and also a wider beam 13.3-dBi gain (49.4° beamwidth) vertically polarized horn antenna) were used at the RX. The maximum measurable path loss was about 160 dB [23], [33]–[35].

38 GHz cellular propagations measurements were conducted in Austin, Texas at the University of Texas main campus [33]. TX locations were placed on four rooftops with different heights, WRW-A (23 meters), ENS-A (36 meters), ENS-B (36 meters), and ECJ (8 meters). A total of 43 TX-RX combinations were measured with up to 12 various antenna configurations for each measurement location [33]. The RX was positioned in a number of LOS, partially obstructed LOS, and NLOS locations representative of an outdoor urban environment including foliage, high-rise buildings, and pedestrian and vehicular traffic. At each receiver location, measurements were acquired using a circular track with 8 equally spaced local area measurement points separated by 45° increments. The radius of the circular track yielded a 10λ separation distance between consecutive points along the circular track. For LOS links, the TX and RX were pointed directly at each other in both azimuth and elevation. The captured PDPs for each complete track measurement were then averaged and a new RX location was selected. NLOS conditions were taken over the circular track and a subsequent 360° azimuth exhaustive signal search was conducted.

B. 38 GHz OUTDOOR MEASUREMENT RESULTS

AOA measurements were shown to be most common when the RX azimuth angle was between −20° and +20° about the boresight of the TX azimuth angle [34]. After examining data for all RX locations for each corresponding TX, it was shown that a lower base station height is more likely to have more links with varying the TX azimuth angle. However, the site specific location of the RX impacts the observed AOA and multipath response. Designing for future base stations will require site specific deployment technologies.

MASSIVELY BROADBAND, IPR2025-01563, Ex.2013, Page 10 of 15

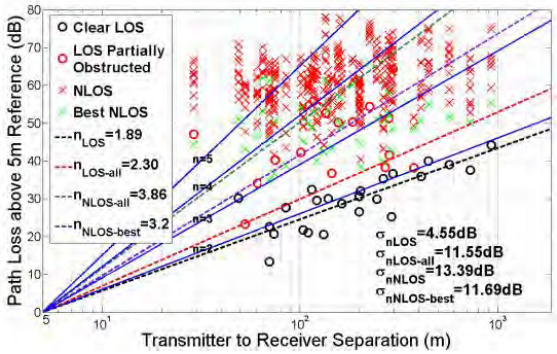

FIGURE 11. Path loss scatter plot using 25dBi Rx antenna at 38 GHz. LOS and NLOS measurements have path loss exponents of 2.30 and 3.86, respectively, while the best NLOS links have a path loss exponent of 3.2 [35].

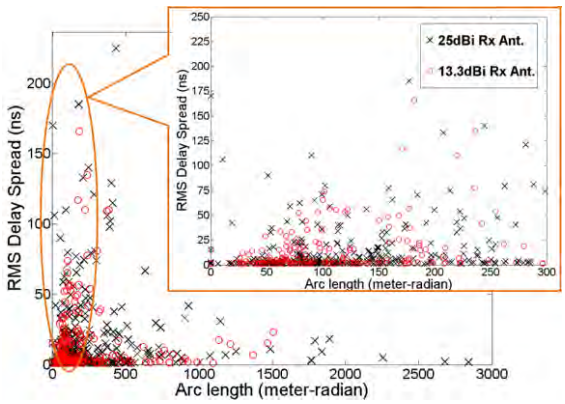

FIGURE 12. RMS delay spread as a function of arc length at 38 GHz. The delay spread decreases over longer arc lengths, which indicates that distance surmounts angle in determining delay spread. Nevertheless, a close-up of low arc lengths shows the angle playing a larger role in determining delay spread [35].

Path loss was determined for 38 GHz in Austin using 13.3 dBi and 25 dBi horn antennas [35]. For all TX locations, measurements at ECJ yielded the highest path loss using both antennas. The LOS PLE for the 25 dBi horn antennas was measured to be n = 2.30 and NLOS PLE was measured to be n = 3.86, as demonstrated in Fig. 11. Compared to measurements in Manhattan at 28 GHz, where the LOS PLE and NLOS PLE were 2.55 and 5.76 respectively, it is clear that PLE at 38 GHz in the light urban environment in Austin is considerably lower.

Analysis of the RMS delay spread at 38 GHz showed sensitivity to antenna gains [23], [33]–[35]. While all cumulative distribution functions (CDF) for LOS and NLOS links are similar, a lower antenna gain was shown to have a higher RMS delay spread, whereas the 25 dBi antenna showed lower delays with greater TX-RX separation. Fig. 12 shows RMS delay spreads for the 25 dBi and 13.3 dBi steerable receiver antennas plotted as a function of arc length.

By conducting an outage study in Austin, we were able to further establish that lower base station heights provide better close-in coverage. By comparing ENS and WRW, 36 and 18 meters in height respectively, we found that no outages occurred within a 200 m cell radius. However, beyond 200 m, 52.8% of locations were outages, 10% of those belong to WRW, and 27.3% to ENS. The coverage radius of 200 m is identical to that measured in New York City, thus suggesting that 200 m is a very achievable cell size for future 5G mm-wave cellular communications systems [23], [33]–[35].

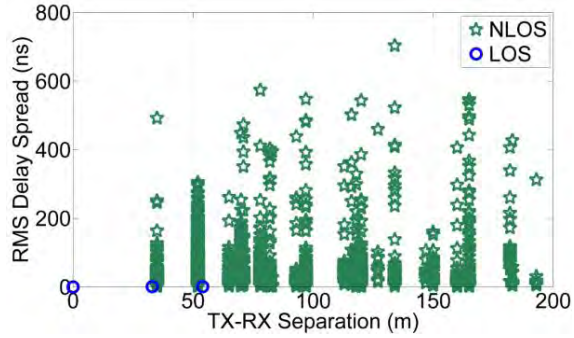

FIGURE 13. RMS delay spread as a function of TX-RX separation for all links using all possible pointing angles at 28 GHz in New York City. The green stars and blue circles denote the RMS delay spread in the NLOS and LOS measurement locations, respectively.

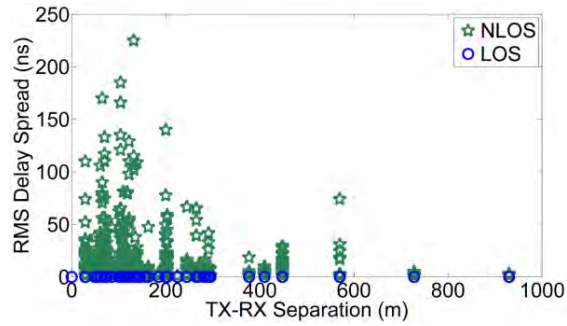

FIGURE 14. RMS delay spread as a function of TX-RX separation for all links using all possible pointing angles at 38 GHz in Austin, Texas. The green stars and blue circles denote the RMS delay spread in the NLOS and LOS environment, respectively.

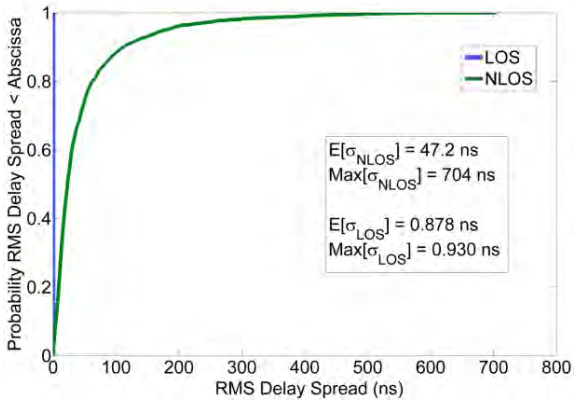

FIGURE 15. Cumulative distribution function (CDF) of the RMS delay spread at 28 GHz measured for all links using all possible pointing angles in the dense urban environment in New York City. The CDFs for LOS and NLOS links over all TX-RX locations are distinguished by the extremely low delay spread in LOS, and extremely mutative spreads in NLOS.

MASSIVELY BROADBAND, IPR2025-01563, Ex.2013, Page 11 of 15

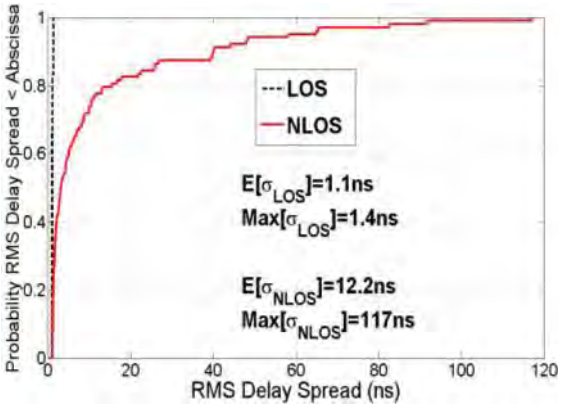

FIGURE 16. CDF of the RMS delay spread of the 38 GHz cellular channel for all links using all possible pointing angles measured in Austin, Texas [23].

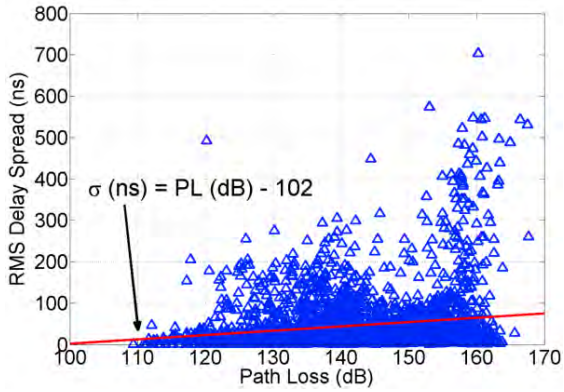

FIGURE 17. RMS delay spread as a function of path loss over all viable pointing angles at 28 GHz in New York City. The blue triangles represent the measured RMS delay spread and the red line denotes a linear fit for the average RMS delay spread.

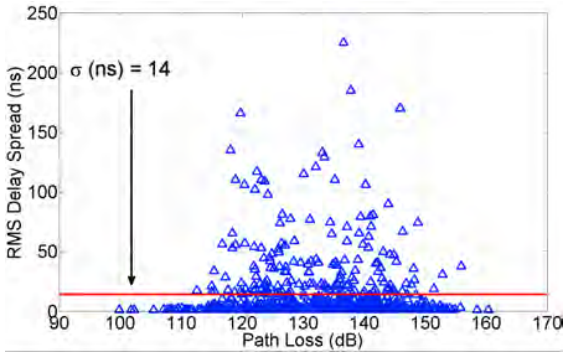

FIGURE 18. RMS delay spread as a function of path loss over all viable pointing angles at 38 GHz in Austin, Texas. The blue triangles represent the measured RMS delay spread, and the red line denotes a linear fit for the average RMS delay spread.

V. STATISTICAL MODELS FOR RMS DELAY SPREAD

Fig. 13 shows the relationship between RMS delay spread and TX-RX separation for the 28 GHz New York City measurements. We note that the maximum value of RMS delay spread appears to be roughly even up to 170-m TX-RX separation, and then decreases for distances greater than 170 m. The delay spread at relatively large TX-RX separations is caused by multipath, which illustrates the highly reflective nature of the dense urban environment in New York City. Yet, when the distance between the TX and RX is too large (close to or exceeding 200 m), the path loss is so great that the power of the transmitted signal declines to zero before reaching the RX, resulting in fewer or no received multipath. The relationship between RMS delay spread and TX-RX separation for 38 GHz Austin measurements is shown in Fig. 14. As seen in Fig. 14, signals in Austin, Texas could still be acquired for TX-RX distances greater than 200 m, and the average RMS delay spread is much lower than that at 28 GHz, thus indicating the relatively sparse urban environment of the UT-Austin campus, where there were fewer buildings to cause obstructions or reflections.

The cumulative distribution function (CDF) of the RMS delay spread at 28 GHz in New York City is illustrated in Fig. 15. In LOS cases, the TX and RX antennas were directly pointed at each other, and very few multipath existed, thus resulting in virtually non-existent RMS delay spread. In NLOS cases, the majority of measured multipath components have RMS delay spreads below 200 ns, while some are as high as 700 ns. As a comparison, the average and maximum RMS delay spread in NLOS cases obtained from 38 GHz cellular measurements in Austin, Texas are 12.2 ns and 117 ns, respectively (see Fig. 16), which are much lower than those at 28 GHz, further demonstrating the propagation conditions in the less cluttered, less dense nature of the urban environment measured in Austin, Texas.

The variation of RMS delay spread versus path loss in NLOS for all TX-RX location combinations at 28 GHz in New York City is displayed in Fig. 17. It is clear from the plot that RMS delay spread increases with path loss, which is similar to the result at 1.9 GHz in [30]. A linear model is adopted to investigate the relationship between RMS delay spread and path loss for the 28 GHz measurements in Manhattan, wher e σ denotes the average RMS delay spread in nanoseconds for a particular value of path loss, and PL is the path loss in decibels ranging from 109 dB to 168 dB. Combined with Fig. 6, the path loss and RMS delay spread models can be utilized to predict outage ranges in microcell mm-wave communication systems. A similar fit is done in Fig. 18 for 38 GHz measurement data from Austin, wherein the average RMS delay spread is found to be virtually identical (14 ns) over the path loss range of 100 dB to 160 dB.

VI. CONCLUSION

Given the worldwide need for cellular spectrum, and the relatively limited amount of research done on mm-wave mobile communications, we have conducted extensive propagation measurement campaigns at 28 GHz and 38 GHz to gain insight on AOA, AOD, RMS delay spread, path loss, and building penetration and reflection characteristics for

MASSIVELY BROADBAND, IPR2025-01563, Ex.2013, Page 12 of 15

the design of future mm-wave cellular systems. This work presents data collected in the urban environments around the University of Texas at Austin (38 GHz) and New York University (28 GHz). Outage studies conducted at 28 GHz and 38 GHz showed that consistent coverage can be achieved by having base stations with a cell-radius of 200 metres. Path loss was larger in New York City than in Austin, due to the nature of the denser urban environment. In New York City, reflection coefficients for outdoor materials were significantly higher, for example, 0.896 for tinted glass, and 0.740 for clear non-tinted glass, compared with those of indoor building materials. Similarly, penetration losses were larger for outdoor materials in New York City. Since signals cannot readily propagate through outdoor building materials, indoor networks will be isolated from outdoor networks and this suggests that data showers, repeaters, and access points may need to be installed for handoffs at entrances of commercial and residential buildings.

By observing the measured path loss and delay spread values from the heavy urban environment of New York City and the light urban environment of Austin, Texas, we found substantial differences in propagation parameters.

Multipath delay spread is found to be much larger in New York City than in Austin, due to the highly reflective nature of the dense urban environment.

Small scale fading, a key factor for the design of urban cellular, has been tested and shows little change in received power and impulse response when highly directional antennas and 400 Mcps signals are used.

The data collected over the course of these measurement campaigns allows for development of statistical channel models for urban environments, and are highly valuable for the development of 5G cellular communications at mm-wave bands in the coming decade.

ACKNOWLEDGMENT

This work was sponsored by Samsung DMC R&D Communications Research Team (CRT), and by Samsung Telecommunications America, LLC. The authors thank George R. MacCartney, Shuai Nie, and Junhong Zhang for their contributions to this project, as well as researchers at Samsung, including W. Roh, D. Hwang, S. Abu-Surru, F. Kahn, and Z. Pi for their on-going interest and support of this work. Hughes Research Laboratory and National Instruments provided equipment used in this work. The authors also thank the NYU administration, NYU Public Safety, and the New York Police Department for their support of these measurements. Measurements were conducted under U.S. FCC experimental license 0040-EX-ML-2012.

REFERENCES

[1] T. S. Rappaport, J. N. Murdock, and F. Gutierrez, "State of the art in 60 GHz integrated circuits & systems for wireless communications," *Proc. IEEE*, vol. 99, no. 8, pp. 1390–1436, Aug. 2011.

[2] Z. Pi and F. Khan, "An introduction to millimeter-wave mobile broadband systems," *IEEE Commun. Mag.*, vol. 49, no. 6, pp. 101–107, Jun. 2011.

[3] *Spatial Channel Model for Multiple Input Multiple Output (MIMO) Simulations (Release 10)*, Standard 3GPP TR 25.996, Mar. 2011.

[4] *Guidelines for Evaluation of Radio Interference Technologies for IMT-Advanced*, Standard ITU-R M.2135, 2008.

[5] T. S. Rappaport, *Wireless Communications: Principles and Practice*, 2nd ed. Englewood Cliffs, NJ, USA: Prentice-Hall, 2002.

[6] L. Xichun, A. Gani, R. Salleh, and O. Zakaria, "The future of mobile wireless communication networks," in *Proc. Int. Conf. Commun. Softw. Netw.*, Feb. 2009, pp. 554–557.

[7] P. Rysavy. (2010). *Transition to 4G: 3GPP Broadband Evolution to IMT-Advanced (4G)* [Online]. Available: http://www.3gamericas.org/documents/Transition%20to%204G-HSPA%20LTE%20Advanced%20Rysavy%202010%20PPT.pdf

[8] Nokia Siemens Networks. (2010). *Long Term HSPA Evolution: Mobile Broadband Evolution Beyond 3GPP Release 10*, Espoo, Finland [Online]. Available: http://lteworld.org/whitepaper/long-term-hspa-evolution-mobile-broadband-evolution-beyond-3gpp-release-10

[9] Ericsson. (2011, Apr.). *LTE-A 4G Solution*, Stockholm, Sweden [Online]. Available: http://www.ericsson.com/news/110415_wp_4g_244188810_c

[10] A. F. Molisch, M. Steinbauer, M. Toeltsch, E. Bonek, and R. Thoma, "Capacity of MIMO systems based on measured wireless channels," *IEEE J. Sel. Areas Commun.*, vol. 20, no. 3, pp. 561–569, Apr. 2002.

[11] J. Fuhl, A. F. Molisch, and E. Bonek, "A unified channel model for mobile radio systems with smart antennas," *Proc. Inst. Electr. Eng.-Radar, Sonar Navigat., Special Issue Antenna Array Process. Tech.*, vol. 145, no. 1, pp. 32–41, Feb. 1998.

[12] S. Rajagopal, S. Abu-Surra, Z. Pi, and F. Khan, "Antenna array design for multi-Gbps mmwave mobile broadband communication," in *Proc. IEEE Global Telecommun. Conf.*, Dec. 2011, pp. 1–6.

[13] Nokia Siemens Networks. (2011). *2020: Beyond 4G: Radio Evolution for the Gigabit Experience*, Espoo, Finland [Online]. Available: http://www.nokiasiemensnetworks.com/file/15036/2020-beyond-4g-radio-evolution-for-the-gigabit-experience

[14] S. Hwang, D. Lyu, and K. Chang, "4G vision and technology development in Korea," in *Proc. IEEE Int. Conf. Commun. Technol.*, vol. 1. Apr. 2003, pp. 26–27.

[15] (2002). *All IP Wireless—All the Way* [Online]. Available: http://www.mobileinfo.com/3G/4G_Sun_MobileIP.htm

[16] K. R. Santhi, V. K. Srivastava, G. SenthilKumaran, and A. Butare, "Goals of true broad band's wireless next wave (4G-5G)," in *Proc. IEEE 58th Veh. Technol. Conf.*, vol. 4. Oct. 2003, pp. 2317–2321.

[17] L. George, "Another generation," *Global Telephony*, vol. 9 no. 2, pp. 1–10, Feb. 2001.

[18] Y. Kim. (2012). *Global Competition, Interconnectivity, Smarter Customers, and Deregulation* [Online]. Available: http://www.3g4g.co.uk/4G/News/20050205.html

[19] L. HyeonWoo, "4G and B4G R&D activities in Korea," in *Proc. Int. Mobile Commun. Symp.*, Sep. 2012, pp. 1–6.

[20] M. Cudak, A. Ghosh, T. Kovarik, R. Ratasuk, T. Thomas, F. Vook, and P. Moorut, "Moving towards mmwave-based beyond-4G (B-4G) Technology," in *Proc. IEEE Veh. Technol. Soc. Conf.*, 2013, pp. 1–17.

[21] Y. Chen, S. De, R. Kernchen, and K. Moessner, "Device discovery in future service platforms through SIP," in *Proc. IEEE Veh. Technol. Conf.*, Sep. 2012, pp. 1–5.

[22] F. Gutierrez, S. Agarwal, K. Parrish, and T. S. Rappaport, "On-chip integrated antenna structures in CMOS for 60 GHz WPAN systems," *IEEE J. Sel. Areas Commun.*, vol. 27, no. 8, pp. 1367–1378, Oct. 2009.

[23] T. S. Rappaport, E. Ben-Dor, J. N. Murdock, and Y. Qiao, "38 GHz and 60 GHz Angle-dependent Propagation for Cellular and peer-to-peer wireless communications," in *Proc. IEEE Int. Conf. Commun.*, Jun. 2012, pp. 4568–4573.

[24] F. Rusek, D. Persson, B. Lau, E. Larsson, T. Marzetta, O. Edfors, and F. Tufvesson, "Scaling up MIMO: Opportunities and challenges with very large arrays," *IEEE Signal Process. Mag.*, vol. 30, no. 1, pp. 40–60, Jan. 2013.

MASSIVELY BROADBAND, IPR2025-01563, Ex.2013, Page 13 of 15

[25] S. Y. Seidel and H. W. Arnold, "Propagation measurements at 28 GHz to investigate the performance of local multipoint distribution service (LMDS)," in *Proc. Global Telecommun. Conf.*, vol. 1. Nov. 1995, pp. 754–757.

[26] Q. Zhao and J. Li, "Rain attenuation in millimeter wave ranges," in *Proc. IEEE Int. Symp. Antennas, Propag. EM Theory*, Oct. 2006, pp. 1–4.

[27] C. R. Anderson and T. S. Rappaport, "In-building wideband partition loss measurements at 2.5 and 60 GHz," *IEEE Trans. Wireless Commun.*, vol. 3, no. 3, pp. 922–928, May 2004.

[28] H. Zhao, R. Mayzus, S. Sun, M. Samimi, J. K. Schulz, Y. Azar, K. Wang, G. N. Wong, F. Gutierrez, Jr., and S. T. Rappaport, "28 GHz millimeter wave cellular communication measurements for reflection and penetration loss in and around buildings in New York City," in *Proc. IEEE Int. Conf. Commun.*, Jun. 2013, pp. 1–6.

[29] G. Durgin, T. S. Rappaport, and H. Xu, "5.85-GHz radio path loss and penetration loss measurements in and around homes and trees," *IEEE Commun. Lett.*, vol. 2, no. 3, pp. 70–72, Mar. 1998.

[30] K. L. Blackard, M. J. Feuerstein, T. S. Rappaport, S. Y. Seidel, and H. H. Xia, "Path loss and delay spread models as functions of antenna height for microcellular system design," in *Proc. IEEE 42nd Veh. Technol. Conf.*, vol. 1. May 1992, pp. 333–337.

[31] Y. Azar, G. N. Wong, K. Wang, R. Mayzus, J. K. Schulz, H. Zhao, F. Gutierrez, D. Hwang, and T. S. Rappaport, "28 GHz propagation measurements for outdoor cellular communications using steerable beam antennas in New York City," in *Proc. IEEE Int. Conf. Commun.*, Jun. 2013, pp. 1–6.

[32] M. Samimi, K. Wang, Y. Azar, G. N. Wong, R. Mayzus, H. Zhao, J. K. Schulz, S. Sun, F. Gutierrez, and T. S. Rappaport, "28 GHz angle of arrival and angle of departure analysis for outdoor cellular communications using steerable-beam antennas in New York City," in *Proc. IEEE Veh. Technol. Conf.*, Jun. 2013, pp. 1–6.

[33] T. S. Rappaport, F. Gutierrez, E. Ben-Dor, J. N. Murdock, Y. Qiao, and J. I. Tamir, "Broadband millimeter wave propagation measurements and models using adaptive beam antennas for outdoor urban cellular communications," *IEEE Trans. Antennas Propag.*, vol. 61, no. 4, pp. 1850–1859, Apr. 2013.

[34] J. N. Murdock, E. Ben-Dor, Y. Qiao, J. I. Tamir, and T. S. Rappaport, "A 38 GHz cellular outage study for an urban campus environment," in *Proc. IEEE Wireless Commun. Netw. Conf.*, Apr. 2012, pp. 3085–3090.

[35] T. S. Rappaport, Y. Qiao, J. I. Tamir, J. N. Murdock, and E. Ben-Dor, "Cellular broadband millimeter wave propagation and angle of arrival for adaptive beam steering systems (invited paper)," in *Proc. IEEE Radio Wireless Symp.*, Jan. 2012, pp. 151–154.

[36] T. S. Rappaport. (2013). *NYU WIRELESS* [Online]. Available: http://nyuwireless.com/

THEODORE S. RAPPAPORT (F'98) received the B.S., M.S., and Ph.D. degrees in electrical engineering from Purdue University, West Lafayette, IN, USA, in 1982, 1984, and 1987, respectively.

He is an Outstanding Electrical and Computer Engineering Alumnus and Distinguished Engineering Alumnus from his alma mater. He holds the David Lee/Ernst Weber Chair in Electrical and Computer Engineering at Polytechnic Institute, New York University (NYU-Poly), Brooklyn, NY, USA, and is a Professor of computer science and Professor of radiology at NYU. In 2012, he founded NYU WIRELESS, a multidisciplinary research center involving NYU's engineering, computer science, and medical schools. Earlier in his career, he founded the Wireless Networking and Communications Group (WNCG), University of Texas at Austin (UT), TX, USA. Prior to UT, he was on the electrical and computer engineering faculty of Virginia Polytechnic Institute and State University, Blacksburg, VA, USA, where he founded the Mobile and Portable Radio Research Group (MPRG), one of the world's first university research and teaching centers dedicated to the wireless communications field. In 1989, he founded TSR Technologies, Inc., Blacksburg, VA, USA, a cellular-radio/personal-communications-services software radio manufacturer that pioneered cellular E-911 and test equipment that he sold in 1993 to what is now CommScope, Inc. In 1995, he founded Wireless Valley Communications Inc., Austin, TX, USA, and a site-specific wireless network design and management firm that was sold in 2005 to Motorola, Inc. He has testified before the U.S. Congress, has served as an international consultant for the ITU, has consulted for more than 30 major telecommunications firms, and works on many national committees pertaining to communications research and technology policy. He is a highly sought-after consultant and technical expert, and serves on the Board of Directors of the Marconi Society. He has authored or co-authored more than 200 technical papers, over 100 U.S. and international patents, and several best-selling technical books.

Dr. Rappaport was elected to the Board of Governors of the IEEE Communications Society (ComSoc) in 2006, and was elected to the Board of Governors of the IEEE Vehicular Technology Society (VTS) in 2008 and 2011.

SHU SUN (S'13) received the B.S. degree in applied physics from Shanghai Jiao Tong University, Shanghai, China, in 2012. She is currently pursuing the Ph.D. degree in electrical engineering with the Polytechnic Institute, New York University (NYU-Poly), Brooklyn, NY, USA.

She joined NYU WIRELESS Research Center in August 2012. She has co-authored two conference publications, and is now working on millimeter-wave propagation measurements campaign for 5G cellular mm-wave communication systems.

RIMMA MAYZUS (S'13) is a sophomore in electrical engineering with Polytechnic Institute, New York University (NYU-Poly), Brooklyn, NY, USA.

She has participated in the 28 GHz mm-wave propagation measurements campaign in 2012, and has co-authored three conference publications.

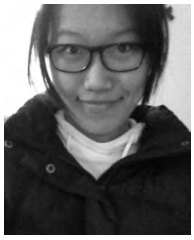

HANG ZHAO (S'13) is a second year undergraduate student in electrical engineering BS/MS program at Polytechnic Institute of New York University (NYU-Poly), Brooklyn, NY, USA. She is currently an Undergraduate Researcher at NYU WIRELESS, and has a first-author conference publication and co-authored two conference publications. Her current research interests include millimeter-wave propagation and semiconductor circuits.

MASSIVELY BROADBAND, IPR2025-01563, Ex.2013, Page 14 of 15

YANIV AZAR (S'12) is currently pursuing both the B.S. and M.S. degrees in electrical engineering with the Polytechnic Institute of New York University (NYU-Poly), Brooklyn, NY, USA.

He has previously worked on 28 GHz millimeter-wave propagation measurement campaign, and has a first-author conference publication and co-authored two conference publications. He currently works on his thesis in the biomedical area.

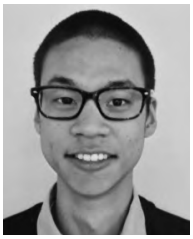

KEVIN WANG (S'13) is a second year undergraduate student in an accelerated Master's program, pursuing an undergraduate degree in computer engineering and a graduate degree in mathematics at Polytechnic Institute of New York University (NYU-Poly), Brooklyn, NY, USA. In 2012, he helped complete the world's first measurements of millimeter-wave propagation. Currently, he is an undergraduate Researcher for NYU WIRELESS building a raytracer for millimeter-wave propagation.

GEORGE N. WONG (S'13) is currently pursuing the Bachelors degrees in physics and mathematics at New York University (NYU), Brooklyn, NY, USA. He works with NYU WIRELESS as a Student Researcher. His current research interests include statistical processing and development of channel models for millimeter-wave and sub-terahertz propagation characteristics, especially the development of ray tracing technologies.

JOCELYN K. SCHULZ (S'13) is currently pursuing the Bachelors degree in electrical engineering and computer science with New York University (NYU), Brooklyn, NY, USA. She is a student Researcher at NYU WIRELESS, working on the development of statistical models and ray tracing software for millimeter-wave frequencies. She was a Software Engineer intern at Google and remains a Google Student Ambassador for NYU in 2012. She was recently accepted into the NYC Turing Fellows Program and will be exploring the exciting startup-life at Knewton this coming summer.

MATHEW SAMIMI (S'13) received the B.S. degree from the Fu Foundation School of Engineering and Applied Sciences of Columbia University in Applied Physics, New York, NY, USA, in 2012. He is currently pursuing the Ph.D. degree in electrical engineering at NYU-Poly, Brooklyn, NY, USA.

He has a first-author conference publication and co-authored another conference publication. He is currently working with Prof. Rappaport on building the next 5G millimeter-wave statistical spatial channel models.

FELIX GUTIERREZ, JR. (S'08) received the B.S. degree in electrical engineering from the University of Texas at Austin (UT), TX, USA, in 2006, the M.S. degree in electrical engineering from Texas A&M University, College Station, TX, USA, in 2008. He is currently pursuing the Ph.D. degree in electrical engineering at UT.

He completed an internship with ETS-Lindgren, Cedar Park, TX, USA, in 2010. He is currently a Visiting Research Scholar with the Polytechnic Institute of New York University (NYU-Poly), Brooklyn, NY, USA. He has worked on millimeter-wave and sub-terahertz semiconductor circuits and antennas for next-generation wireless communications.

MASSIVELY BROADBAND, IPR2025-01563, Ex.2013, Page 15 of 15